Research in Pharmaceutical Sciences, August 2024; 19(4): 459-474
Received: 14-05-2023
Peer Reviewed: 18-06-2023
Revised: 30-08-2023
Accepted: 12-08-2024
Published: 19-08-2024

School of Pharmacy & Pharmaceutical Sciences
Isfahan University of Medical Sciences

Original Article

Mesoporous silica and alumina nanoparticles to improve drug delivery of pioglitazone on diabetic type 1 nephropathy in rats

Jaleh Varshosaz[1,2], Saeedeh Ahmadipour[3,4,*], and Armin Dezhangfard[5]

[1]*Department of Pharmaceutics, School of Pharmacy and Pharmaceutical Sciences, Isfahan University of Medical Sciences, Isfahan, Iran.*
[2]*Novel Drug Delivery Systems Research Center, School of Pharmacy and Pharmaceutical Sciences, Isfahan University of Medical Sciences, Isfahan, Iran.*
[3]*Department of Pharmaceutics, School of Pharmacy, Lorestan University of Medical Sciences, Khorramabad, Iran.*
[4]*Razi Herbal Medicines Research Center, Lorestan University of Medical Sciences, Khorramabad, Iran.*
[5]*Student Research Committee, Lorestan University of Medical Sciences, Khorramabad, Iran.*

Abstract

Background and purpose: Diabetic nephropathy leads to end-stage renal disease. The present study aimed to evaluate the prophylactic effect of pioglitazone-loaded mesoporous silica and alumina scaffold on renal function and the underlying mechanisms in streptozotocin-induced diabetic rats.
Experimental approach: The mesoporous nanoparticles were synthesized by chemical methods from tetraethylorthosilicate and aluminum isopropoxide and characterized by Fourier transform infrared spectroscopy, X-ray diffraction, and scanning electron microscopy. The soaking method was applied to load pioglitazone into the mesoporous silica and alumina. Subsequently, the most capable formulation was evaluated for lipid profile, blood glucose, renal function biomarkers, malondialdehyde, and kidney histopathological changes in diabetic rats.
Findings/Results: Pioglitazone loaded in the mesoporous included a superior release of about 80%. No interaction was observed in Fourier transform infrared spectroscopy and X-ray diffraction was shown crystalline. Scanning electron microscopy showed the size of the nanometer in the range of 100 - 300 nm. Mesoporous silica containing the drug significantly decreased urinary parameters, triglycerides, low-density lipoprotein, blood urea nitrogen, blood glucose, malondialdehyde, and creatinine. In addition, it showed increased high-density lipoprotein, significantly. The renal histopathological changes indicated improvement compared with the untreated diabetic group.
Conclusion and implications: It was concluded that the mesoporous was potent to serve as a promising drug carrier and a platform aimed at the delivery of poorly water-soluble drugs for improving oral bioavailability. Furthermore, it has the potential to provide a beneficial effect on the changes in diabetic parameters.

Keywords: Diabetic nephropathy; Mesoporous alumina; Mesoporous silica; Pioglitazone; Poorly water-soluble.

INTRODUCTION

The global prevalence of impaired glucose tolerance is estimated to represent 374 million in 2019, and it is anticipated to reach 454 million by 2030 and 548 million by 2045 (1). Complications in the eyes, heart, nerves, and kidneys in diabetic patients lead to reduced quality of life and increased mortality and morbidity rates. Diabetic nephropathy (DN) exists in more than 40% of patients with diabetes (2). Chronic kidney failures results in DN, leading to chronic kidney disease and end-stage renal disease, and it ultimately causes fatality (3). The characteristic features of DN include severe albuminuria and structural modifications like the results of end-stage renal disease requiring dialysis or transplantation which is an expanding medical issue all over the world (4).

*Corresponding author: S. Ahmadipour
Tel: +98-6633120242, Fax: +98-6633120240
Email: saeedehahmadipour@gmail.com

Access this article online	
	Website: http://rps.mui.ac.ir
	DOI: 10.4103/RPS.RPS_65_23

The beginning phase of diabetic mellitus is represented by renal hyperfiltration, which advances the possible improvement of DN (5).

Thiazolidinediones (TZDs) as pharmacological agents decrease insulin resistance directly through the activation of peroxisome proliferator-activated receptor gamma (PPARγ) (6). On the other hand, both insulin resistance and low-grade systemic inflammation are associated with atherosclerotic plaque formation. Therefore, pioglitazone improves insulin resistance and reduces systemic inflammation (7,8).

PPARγ plays crucial roles in the differentiation of adipocytes, lipid, and carbohydrate metabolism *via* the transcriptional regulation of various genes (9).

Pioglitazone is a highly lipophilic class II drug with poor aqueous solubility (5.32 µg/mL in distilled water at 27 °C). It possesses low oral bioavailability (10), which may adversely affect its dissolution rate (11). The dose of pioglitazone ranged from 15 to 45 mg/day (12).

Mesoporous materials have positive features such as the wide surface area and high porosities, outstanding thermal properties, mechanical stability (13), chemically inert, easy surface modification, the extraordinary potential for drug uptake and accumulation inside pore channels (14), impressive mesoporous structure, flexible pore measurement (15), the better control of accumulation and the capacity of mesoporous channels to change the crystalline state of the drug into an amorphous state (14). Therefore, they are utilized in many applications, including drug delivery systems (13).

Consequently, utilizing mesoporous materials as medication transporters can improve the dissolution rate and stability of poorly water-soluble medications. The current study represented a way to deal with creating and assessing pioglitazone-loaded mesoporous alumina and silica for improving the solubility and dissolubility of pioglitazone. Also, the most capable formulation was tested to investigate the effect of pioglitazone on renal function and kidney histopathological changes during the progression of diabetic nephropathy in type 1 diabetic rats. Pictorial illustration of the whole procedure of producing the mesoporous scaffold and its evaluation are shown in Fig.1.

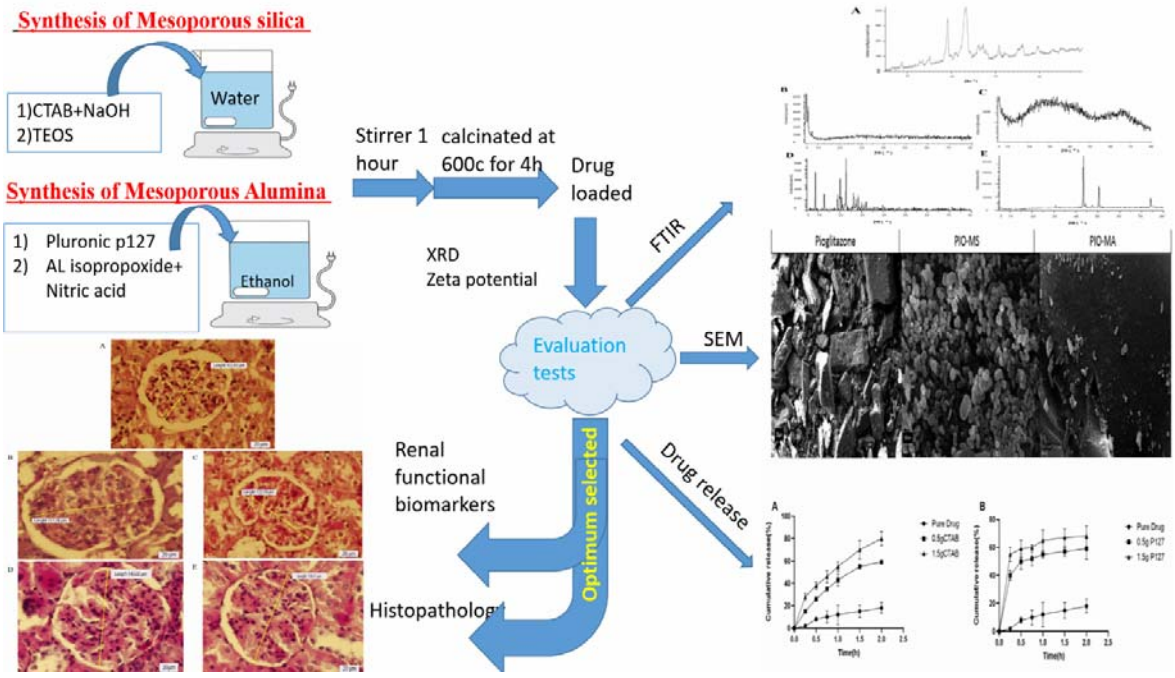

Fig. 1. Schematic representation of the procedure of production the mesoporous silica, alumina, and evaluation tests.

MATERIALS AND METHODS

Chemicals and agents

Pioglitazone was freely provided by Farabi Pharmaceutical Company (Iran). Pluronic P127, tetraethyl orthosilicate (TEOS), cetyltrimethylammonium bromide (CTAB), and aluminum isopropoxide were acquired from Sigma-Aldrich Company (USA). Methanol and ethanol were purchased from Merck Company (USA) and Razi Company (Iran), respectively. Streptozotocin (STZ) and the diagnostic kit of malondialdehyde (MDA) were obtained from Enzo Life Sciences Company (USA). A glucometer, Accu-check Go, was taken from Roche Diagnostics (Meylan, France). Diagnostic kits including creatinine (Cr), blood urea nitrogen (BUN), triglycerides (TG), low-density lipoprotein (LDL), and high-density lipoprotein (HDL) were provided by Pars Aazmoon Company (Iran).

Synthesis of mesoporous silica

To synthesize mesoporous silica (MS) the different amounts of CTAB (0.5 and 1.5 g) were added to 120 mL of distilled water containing 1.75 mL of NaOH 2 M and stirred. TEOS (2.335 g) was rapidly added *via* injection to clear the solution (16). A white precipitate was observed after constant stirring at 500 rpm. Then, the products were isolated by hot filtration and washed 3 times with the total volume of water and methanol (5 mL, 1:1). For 1 g of the prepared sample, acid extraction was performed using a mixture of 100 mL of methanol and 1 mL of HCl at 60 °C for 6 h using a hot plate stirrer. Surfactant removed from solid products was washed with methanol and water mixture (1:1) and centrifuged (D-7200 Tuttlingen, Hettich Company, Germany) at 5000 rpm for 5 min. The prepared mesoporous was placed in a furnace at 600 °C for 4 - 5 h to ensure the surfactant removal.

Synthesis of mesoporous alumina

To synthesize the scaffold of mesoporous alumina (MA) the different amounts of Pluronic (P127, 0.5 and 1.5 g) were dissolved in 20 mL of ethanol, and stirred at room temperature for 1 h. Then, 1.0213 and 2.039 g of 98% aluminum isopropoxide were added, followed by 1.6 mL of 70% nitric acid. The prepared mixtures were continuously stirred at room temperature for 12 h. Surfactant evaporation was performed at 600 °C for 4 h in the furnace (17). After 2 days of aging at room temperature (27 °C), a light yellow solid was obtained.

Drug loading

The solvent deposition method was applied to load the drug. First, 20 mg of pioglitazone was dissolved in 20 mL of ethanol in a sealed glass bottle; then, a certain amount of the fabricated MS and MA was added into the solution with the silica/drug mass ratio of 2:3 (w:w) (18). After gently stirring at room temperature overnight, the mixture was dried at 35 °C. The drug-loaded MS and MA were heated to 55 °C for 30 min and placed under reduced pressure at 40 °C for another 48 h to ensure the complete removal of ethanol. The actual drug loadings were ascertained by extracting an accurately weighed number of drug-loaded composites with ethanol, followed by determining drug content using ultraviolet spectroscopy of 269 nm. All measurements were carried out in triplicate. The drug entrapment efficiency (EE) was calculated using the following equation:

$$\text{EE (\%)} \frac{\text{Total drug} - \text{free drug}}{\text{Total drug}} \times 100$$

Fourier transform infrared spectroscopy

Fourier transform infrared (FTIR) spectroscopy represents an efficient tool for identifying types of chemical bonds and functional groups in a molecule by producing an infrared absorption spectrum. Samples were mixed with potassium bromide powder and compressed to a 12-mm disc by a hydraulic press at a 10-ton compression force for 30 s. Afterward, a spectral region of 400 - 4000 cm^{-1} was scanned (18).

X-ray diffraction

X-ray diffraction (XRD) is a conventional technique to study and characterize crystalline materials (11). The sample holder cavity of the XRD was filled with the ground sample powder and then smoothed with a spatula. The XRD patterns of pioglitazone samples were obtained using the XRD instrument (Bruker, Germany).

Release studies

The pioglitazone released amounts from the nanoparticles were measured in phosphate-buffered saline (PBS, 0.01 M, pH 6.0) at 37 °C. Dialysis bags (cut-off 12 KDa, Membra-Cel Viskase, USA) were filled with 1 mL of nanoparticle dispersion and sunk into PBS to separate the free drug for about 15 min. Afterward, the bags were transferred to 20 mL of fresh PBS medium while stirring at a velocity of 500 rpm. Then, for 2 h at the distinctive periods, the concentration of the drug leaked in the medium was assessed by a UV spectrophotometer at 269 nm. Blank samples were utilized with the identical method, and each absorbance of the sample was subtracted from the drug sample. All measurements were carried out in triplicate.

Assessment of particle size and zeta potential of nanoparticles

The mean particle size (z - average) and zeta potential of MS and MA were measured with a Zetasizer (Zen 3600, Malvern Instrument Ltd., Worcestershire, UK) in deionized water at 25 °C. One mL of samples was sonicated in a water bath sonication and then measured with Zetasizer. All measurements were carried out in triplicate.

Scanning electron microscopy

Scanning electron microscopy (SEM) (XL 30, Philips Company, Netherland) examined the morphology of synthesized MS and MA. A few drops of the MA and MS-containing drug solution were poured onto the lamellar and dried at room temperature. The samples were covered with copper bases and gold-plated, and then observed using an electron microscope for their morphology (19).

Animal model

Male Wister rats weighing 200-250 g provided from the Lorestan University of Medical Sciences were applied in the study. The animals were housed in the animal room of Lorestan Medical Faculty under standard conditions such as a temperature of 18 - 22 °C, 55 - 65% relative humidity, 12-h light/12-h dark cycle, and free access to water and a standard food regimen. The animal studies were done according to the Ethics Committee of Lorestan University of Medical Sciences (Ethic No. IR.LUMS.REC.1400.211).

The animals were categorized into 5 groups (n = 6) as follows: (A) non-diabetic group (normal), (B) diabetic group without any treatment (control), (C) diabetic group receiving subcutaneous NPH insulin (3 units/kg/day) (insulin), (D) diabetic group receiving the only pioglitazone solution (30 mg/Kg/day) by gavage (PIO), and (E) diabetic group receiving solution containing pioglitazone loaded in mesoporous (30 mg/Kg/day) by gavage (PIO-MS).

STZ dissolved in 50 mM sodium citrate buffer (pH 4.5) was injected in a single dose of 50 mg/kg (intraperitoneally) to induce a diabetic model (20). For preparing the buffer solution with pH 4.5, 0.244 g of sodium citrate was dissolved in 10 mL of distilled water and nitric acid (0.5 g/1 mL) to make the buffer and then was tested with a pH meter (21). Five days after the STZ injection, blood samples were drawn from the rats' tail veins, and glycemic measurements were performed by the glucometer to determine whether the rats were diabetic. Rats with blood glucose levels > 300 mg/dL were considered diabetic (21) and included in the study. To ensure the induction of diabetic nephropathy, the animals did not receive any treatments for 4 weeks after the injection of STZ. They were then subjected to the experimental groups. Afterward, the animals received the respective treatments for an additional 4 weeks. The total duration of the study was considered 8 weeks. The cages were cleaned and the water bottles were changed during the time.

Sample preparation

The parameters including body weight, water intake, and 24-h urine output in the 0^{th}, 4^{th}, and 8^{th} weeks after STZ injection were measured. For urine collection, the rats were individually kept in the metabolic cages for 24 h. For measuring blood chemical parameters 0, 4, and 8 weeks after STZ injection, the rats were anesthetized by ether, and the blood samples were taken from femoral vein.

Measurement of urinary and blood parameters

The blood samples were centrifuged at 3000 rpm for 15 min (D-7200, Hettich, Tuttlingen, Germany), and the supernatants were used to measure Cr, BUN, LDL, HDL, TG, and MDA. The urine samples were measured for urine volume, sodium, and potassium. The measurements were performed based on the instructions written in the diagnostic kits. In addition, the fasting blood glucose (FBG) levels were determined by the glucometer at 0, 4, and 8 weeks after STZ injection *via* the blood tail vein.

Histological analysis

At the end of 8 weeks, the animals were killed, and the left kidney tissues removed were fixed by immersion in 10% formalin solution for at least 24 h. The specimens were dehydrated and embedded in paraffin blocks. The sections were made perpendicular of the defects and decreased to a 5-µm thickness using micro grinding. The specimens were stained by hematoxylin and eosin (H & E) method according to the general protocol (20). The glomerular cross-sectional area of 20 glomeruli randomly selected in each rat was measured by scanning the outer cortex with a computer-aided manipulator. Renal tissue samples were examined for histopathological parameters such as changes in glomerular and Bowman capsule sizes, the attachment of glomerular tubule to Bowman capsule, mesangial matrix, and capillary wall thickening. A professional pathologist in a single-blind procedure histologically assessed the specimens using a light microscope (Olympus, Tokyo, Japan).

Statistical analysis

SPSS statistical program (version 19) was used to examine the mean differences among the groups. The data were expressed as mean ± SD. Paired T-test was used to compare urinary and blood parameters, and body weight among 0, 4, and 8 weeks in each group. To analyze data among groups one-way analysis of variance (ANOVA) followed by the Tukey post-test was applied. GraphPad Prism software (version 8) was used for the dissolution of pioglitazone analysis and the generation of dissolution graphs. $P < 0.05$ was considered the significant difference.

RESULTS

Characterization of the MA and MS

FTIR study

The IR spectrum of the pure drug showed that the presence of a peak at 846.72 cm^{-1} represented aromatic C-H, 1153 cm^{-1} C-O-H deformation, 1240.18 and 1315.4 cm^{-1} corresponded to the C-CH3, 1510.21 cm^{-1} corresponded to the S=O, and 1683.21 cm^{-1} due to NH-C=O group. To investigate the interactions of materials, formulations containing more surfactant were investigated (1.5 g CTAB and 1.5 g P127).

As shown in Fig. 2A, the strong absorbance at 1082 cm^{-1} was attributed to the silica's Si-O stretch, and the absorbance at 1635 and 3419 cm^{-1} was assigned to the surface hydroxyl groups of MS. The signals corresponding to the Si-OH represented a signal at 810 cm^{-1}, as depicted in Fig. 2A. To clarify, the FTIR spectrum of pioglitazone (pure drug) was compared with the FTIR spectrum of formulations containing pioglitazone illustrated in Fig. 2B. The comparison noted the same peaks of pioglitazone in the spectra. Figure 2C showed that broadband 3400 - 3500 cm^{-1} was assigned to the stretching vibration of the OH group bonded to Al cation, and the peak of 1606 cm^{-1} corresponded to water hydration. The shoulder band 1400 cm^{-1} corresponded to the $-NO_3$ group from HNO_3 added for acid treatment, while the peak at 400 - 500 cm^{-1} assigned the bending vibrations of Al-O. Figure. 2D showed that drug-related peaks remained unchanged after aluminum loading (PIO-MA). In addition, no interactions were observed between pioglitazone and MS or MA (Fig. 2B and 2D).

Powder XRD of MA and MS

The drug-loaded sample was recorded to decide whether the XRD pattern of the drug was considered crystalline. The XRD pattern of the drug showed that it was highly crystalline, as demonstrated by the various sharp peaks (Fig. 3A). To check the crystallinity, formulations containing more surfactant were investigated (1.5 g CTAB and 1.5 g P127).

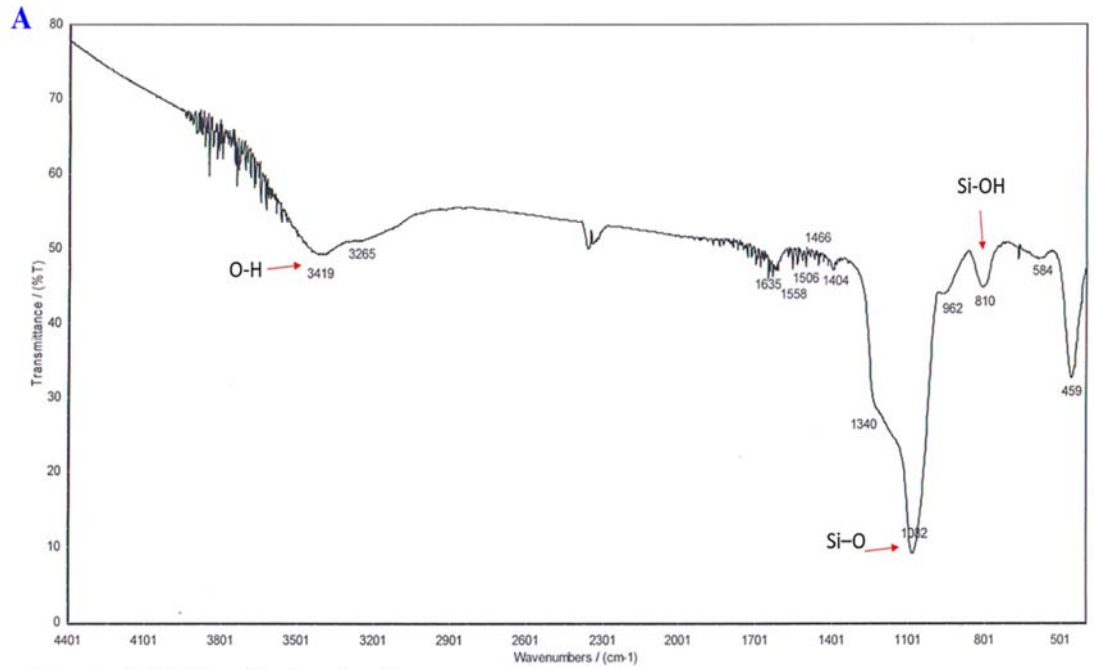

Instrument model=WQF-510 resolution=4 scan times=10

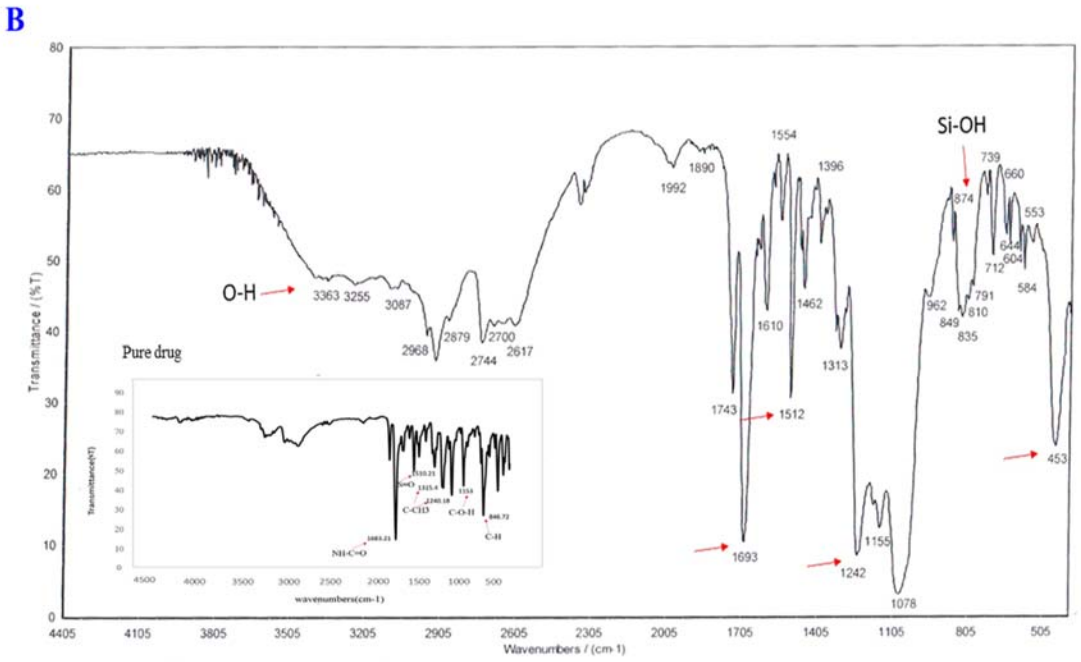

Instrument model=WQF-510 resolution=4 scan times=10

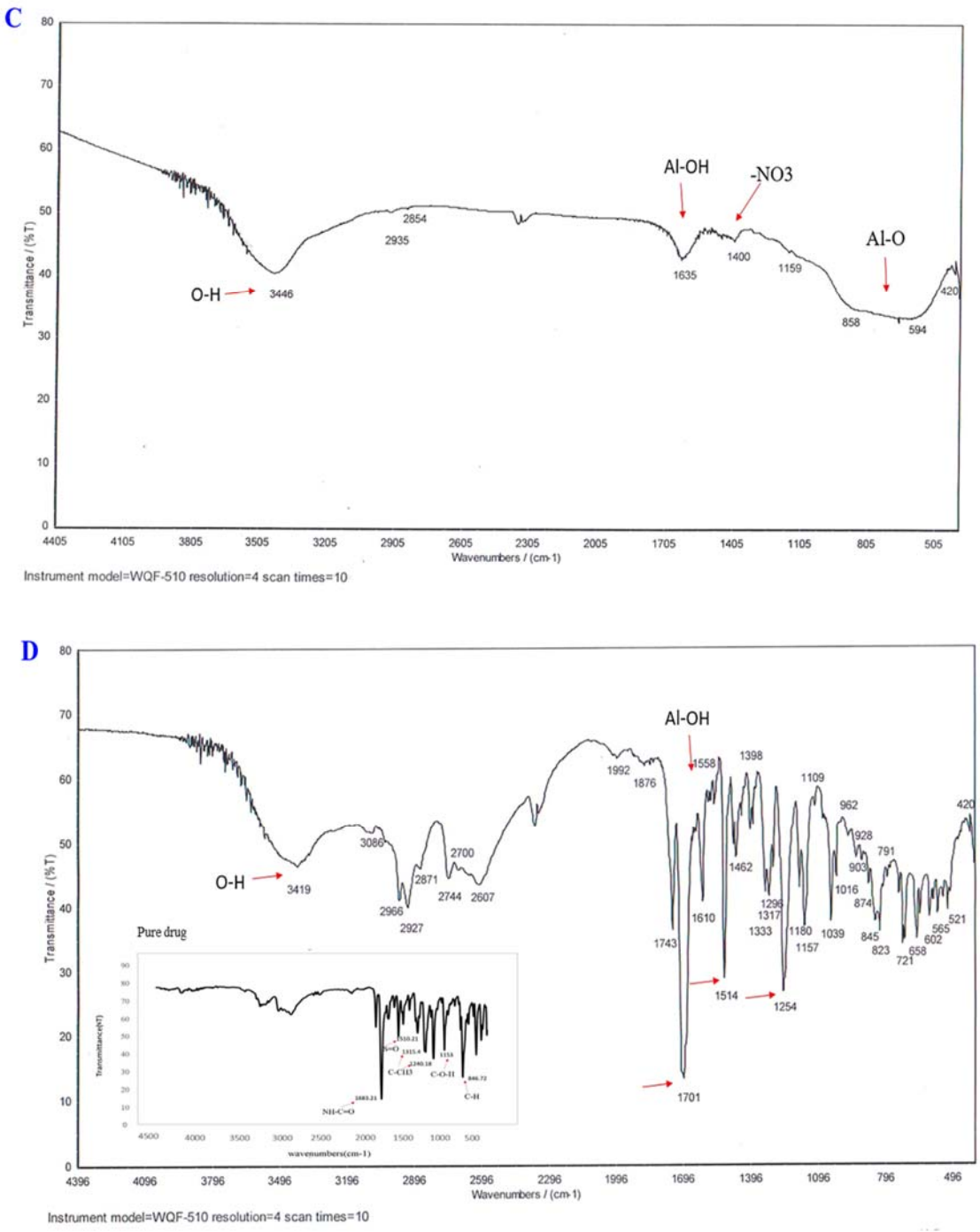

Fig. 2. FTIR spectrum of the (A) MS; (B) PIO-MS; (C) MA; (D) PIO-MA. MS, Mesoporous silica; MA, mesoporous alumina; PIO-MS, pioglitazone-loaded mesoporous silica; PIO-MA, pioglitazone-loaded mesoporous alumina.

The peaks represented that the silica (Fig. 3B) and aluminum (Fig. 3C) structures were amorphous. After drug loading, nanoparticles became crystalline (Fig. 3D and 3E), and PIO-MS nanoparticles showed more sharp peaks and crystallinity than PIO-MA (Fig. 3D and 3E).

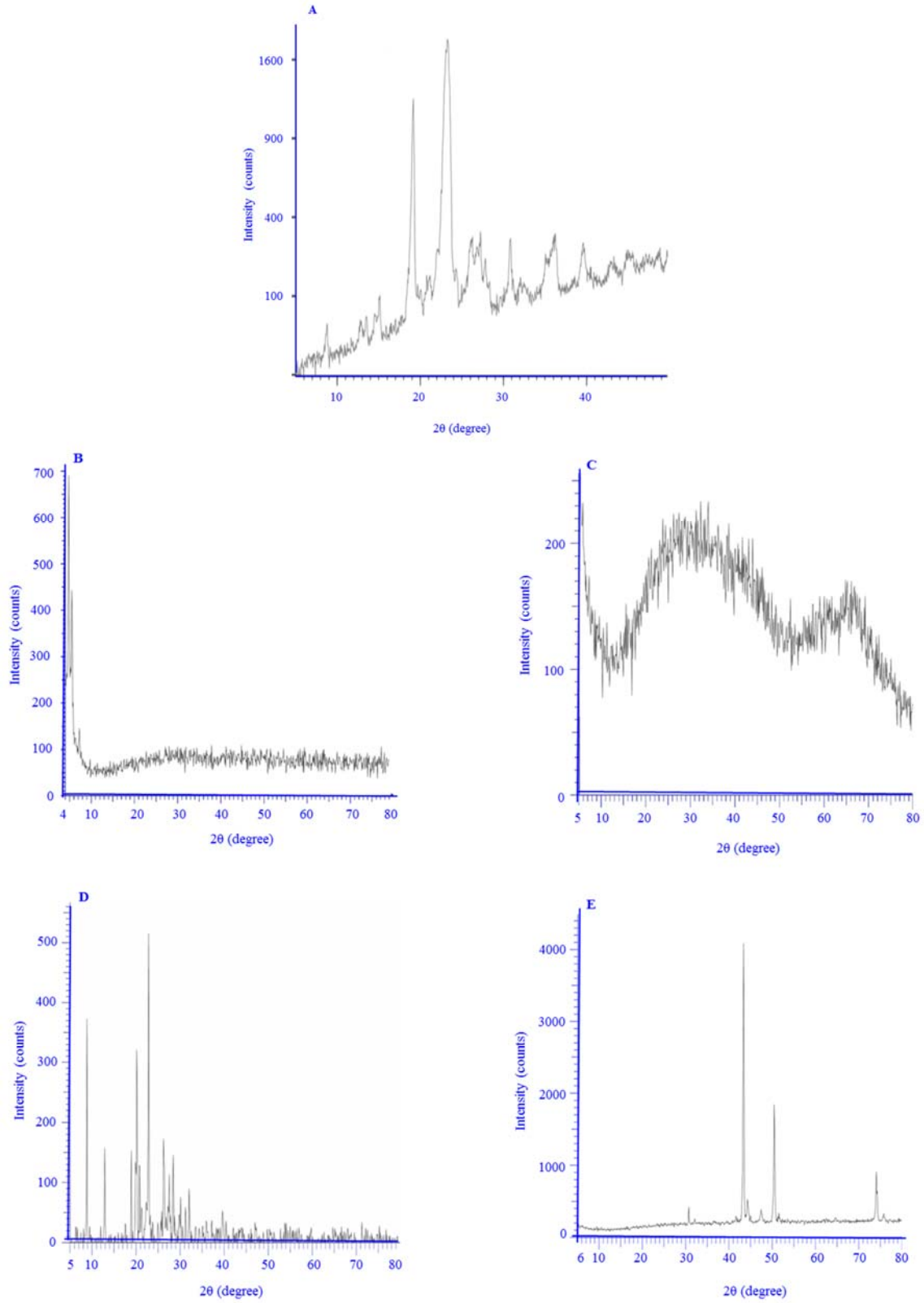

Fig. 3. XRD spectrum of (A) pioglitazone; (B) MS; (C) MA; (D) PIO-MS; and (E) PIO-MA. MS, Mesoporous silica; MA, mesoporous alumina; PIO-MS, pioglitazone-loaded mesoporous silica; PIO-MA, pioglitazone-loaded mesoporous alumina.

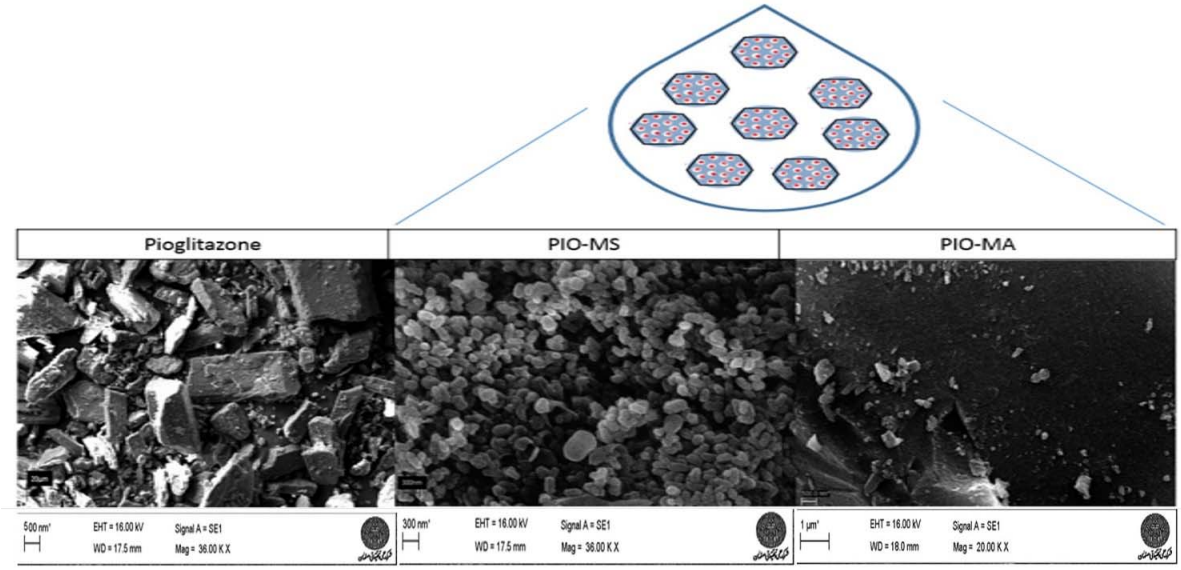

Fig. 4. Scanning electron microscopy from pioglitazone, PIO-MS, and PIO-MA. MS, Mesoporous silica; MA, mesoporous alumina; PIO-MS, pioglitazone-loaded mesoporous silica; PIO-MA, pioglitazone-loaded mesoporous alumina.

Table 1. Particle size, zeta potential and entrapment efficiency of MS and MA.

	MS	MA
Particle size (nm)	178.2 ± 2.36	254.2 ± 3.21
PDI	0.355 ± 0.02	0.345 ± 0.01
Zeta potential (mv)	- 36 ± 2.4	- 38.2 ± 3.1
Entrapment efficiency (%)	(0.5 g CTAB) 32 ± 5.3 (1.5 g CTAB) 58 ± 6.7	(0.5 g P127) 19 ± 3.8 (1.5 g P127) 39 ± 4.3

Data were shown as Mean ± SD, n = 3. MS, Mesoporous silica; MA, mesoporous alumina; PDI, polydispersity index; CTAB. cetyltrimethylammonium bromide; P127, pluronic 127.

Scanning electron microscopy

Figure 4 exhibited the morphology of samples on SEM. SEM analyzed the morphology and particle size of pioglitazone (Fig. 4A), PIO-MS (Fig. 4B), and PIO-MA (Fig. 4C). SEM micrographs showed that PIO-MS had a nearly monodispersed spherical shape with a minimum size of 100 nm and a maximum size of almost 250 nm (Fig.4.B). The morphology of synthesized PIO-MA samples was permeable, with smooth surfaces at the size of around 200-300 nm (Fig. 4C). While the pure drug was observed in the micro range with various sizes (Fig. 4A).

Drug loading and dissolution quantification

The maximum drug loading by UV method was 19 ± 3.8% for MA (0.5 g P127) and 39 ± 4.3% for MA (1.5 g P127). The maximum drug loading was measured at 32 ± 5.3% for MS (0.5 g CTAB) and 58 ± 6.7% for MS (1.5 g CTAB) (Table 1).

In the dissolution study of PIO and PIO-MA, an initial burst release pattern of the drug from the surface was observed for PIO-MA in the first 15 min including 55 ± 7.13% for 1.5 g P127 and 40 ± 3.3% for 0.5 g P127. The release continued to reach around 68 ± 5.2% for 1.5 g P127 and 59 ± 5.6% for 0.5 g P127 at 2 h (Fig. 5B). On the other hand, PIO loaded in MS showed a higher release. The release was at around 15 ± 1.4% for 0.5 g CTAB and 28 ± 1.6% for 1.5 g CTAB in the first 15 min. In continue, it reached around 80 ± 6.21% for 1.5 g CTAB and 59 ± 4.4% for 0.5 g CTAB at 2 h (Fig. 5A). The release of pure pioglitazone was up 18 ± 1.6% at the end up 2 h (Fig. 5).

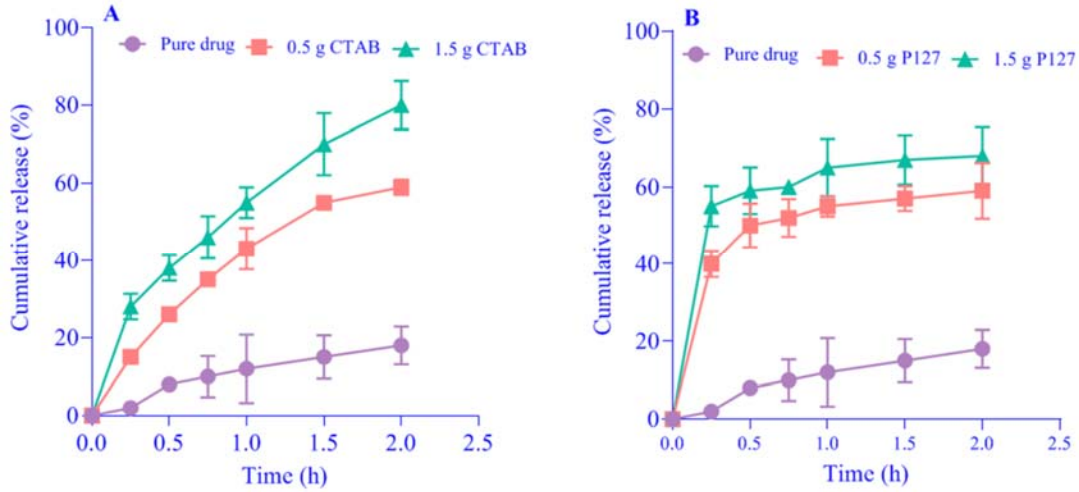

Fig. 5. Dissolution graph of (A) pioglitazone as pure drug and pioglitazone loaded in MS nanoparticles made with 0.5 and 1.5 g CTAB; (B) pioglitazone as pure drug and pioglitazone loaded in MA nanoparticles made with 0.5 and 1.5 g P127. Data were shown as Mean ± SD, n=3. MS, Mesoporous silica; MA, mesoporous alumina; PIO-MS, pioglitazone-loaded mesoporous silica; PIO-MA, pioglitazone-loaded mesoporous alumina; CTAB, cetyltrimethylammonium bromide; P127, pluronic 127.

Particle size and zeta potential

Because the drug release results from the nanoparticles showed that the formulations containing more surfactant loaded and released more drugs, the particle size and potential measurements were performed on the nanoparticles. The obtained particle size of MS and MA indicated 178.2 ± ٢,٣٦ nm (1.5 g CTAB) and 254.2 ± 3.21 nm (1.5 g P127), respectively (Table 1).

The polydispersity indices (PDI) of the nanoparticles studied in the current research were 0.35 ± 0.02 (1.5 g CTAB) and 0.34 ± 0.01 (1.5 g P127) for MS and MA, respectively.

Zeta-potential value was negative in all samples, including 31 - 40 Mv for MS (1.5 g CTAB) and 30 - 44 Mv for MA (1.5 g P127).

Factors examined in animals

According to the results, MS had a smaller size and more loading, and the drug could be released for a longer time. Therefore, only MS loaded with the drug (PIO-MS, 1.5 g CTAB) was used in all animal stages to check the effectiveness.

Physical parameters

Data were obtained at the 0th, 4th, and 8th weeks after STZ injection. The body weight in diabetic rats without treatment was notably lower than the other groups in the 8th week. Also, the body weight remarkably was different between before and after treatment in treated groups. Body weight in the normal group increased dramatically in the 8th week compared with the 4th week, and weight gain increased considerably in the insulin group compared with the control group (Table 2).

Urinary parameters

The results of various urine parameters for each group were presented in Table 2. Urine volume in the normal group did not significantly change throughout the experiment. After STZ injection, urine volume was significantly increased in all diabetic groups before treatment (4th week). The control group had more urine volume compared with the normal group. Urine volume decreased in insulin and PIO-MS treated groups compared with before treatment (4th week) as well as in comparison to the PIO group, significantly.

The urinary potassium and sodium concentrations were significantly higher in the control, insulin, and PIO groups than in the normal group, significantly. The insulin and PIO-MS groups considerably exhibited decreasing in the urinary concentrations than before treatment (4th week). Although, such observation was not seen in the control and PIO groups.

Table 2. Urinary parameters and body weight at the 0th, 4th and 8th weeks in the experimental groups.

Group	Time (week)	Body weight (g)	Urine volume (mL/day)	Na (mEq/day)	K (mEq/day)
Group A (normal)	0	190.1 ± 3.21	15.1 ± 1.3	0.54 ± 0.05	1.1 ± 0.03
	4	201.5 ± 1.15	16.62 ± 0.05	0.62 ± 0.02	1.45 ± 0.01
	8	270.8 ± 2.14$^{*\#b}$	12.25 ± 1.17^{bcde}	1.24 ± 0.01^{bcde}	1.65 ± 0.03^{bcde}
Group B (control)	0	187.1 ± 5.11	12.3 ± 1.11	0.33 ± 0.02	1.03 ± 0.04
	4	208.5 ± 3.02	104.25 ± 2.04$^{\#}$	3.32 ± 0.21$^{\#}$	4.31 ± 0.31$^{\#}$
	8	170.51 ± 6.11^{acde}	99.25 ± 3.11$^{\#acd}$	4.89 ± 0.41$^{\#ace}$	4.39± 0.43$^{\#ace}$
Group C (insulin)	0	180.4 ± 5.21	16.2 ± 2.23	0.34 ± 0.02	1.5 ± 0.01
	4	195.20 ± 3.21	93.84 ± 1.51$^{\#}$	3.33 ± 0.01$^{\#}$	4.45 ± 0.41$^{\#}$
	8	264.5 ± 2.05$^{*\#bde}$	56.21 ± 2.02$^{*\#abd}$	1.41 ± 0.24^{*abd}	2.02 ± 0.23*abd
Group D (PIO)	0	218.2 ± 4.22	14.2 ± 2.12	0.31 ± 0.01	1.22 ± 0.01
	4	228.3 ± 6.11	92.62± 3.5$^{\#}$	3.83 ± 0.22$^{\#}$	3.71 ± 0.12$^{\#}$
	8	252.12 ± 5.04^{*ab}	91.37 ± 3.41$^{\#acd}$	3.88 ± 0.13$^{\#ace}$	3.93± 0.01#ace
Group E (PIO-MS)	0	178.4 ± 4.34	15.1 ± 0.61	0.05 ± 0.01	1.11 ± 0.01
	4	202.21 ± 4.25	94.25 ± 3.33$^{\#}$	3.84 ± 0.41$^{\#}$	3.46 ± 0.24#
	8	244.8 ± 4.04$^{*\#ab}$	68.23 ± 2.21$^{*\#abd}$	1.84 ± 0.01^{*bd}	1.03 ± 0.03*bd

Data were shown as Mean ± SD. Paired T-Test was used to compare differences between weeks in each group. $^{\#}P < 0.05$ shows significant difference compared to the 0th week; $^{*}P < 0.05$ versus the 4th week. ANOVA was used to compare differences in the 8th week among groups. $^{a}P < 0.05$ indicates significant difference compared to normal group; $^{b}P < 0.05$ versus control group; $^{c}P < 0.05$ versus insulin group (positive control); $^{d}P < 0.05$ versus PIO group; $^{e}P < 0.05$ versus PIO-MS group. PIO, Pioglitazone; PIO-MS, pioglitazone-loaded mesoporous silica.

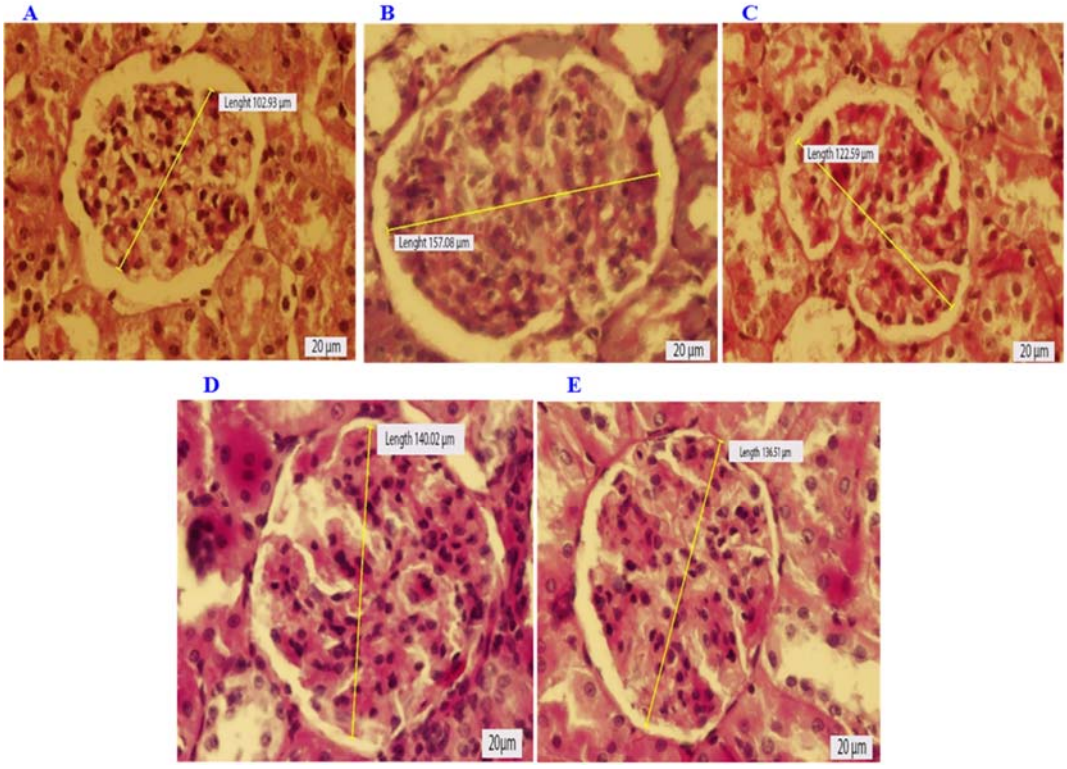

Fig. 6. Renal biopsy specimens stained by hematoxylin and eosin staining (magnification ×400). (A) Normal group; (B) control; (C) insulin (positive control); (D) PIO; (E) PIO-MS. MS, Mesoporous silica; MA, mesoporous alumina; PIO-MS, pioglitazone-loaded mesoporous silica; PIO-MA, pioglitazone-loaded mesoporous alumina.

Blood biochemical parameters

The various biochemical results for each group were presented in Table 3. Results showed that the amounts of blood glucose, BUN, Cr, LDL, TG, and MDA notably increased, and the level of HDL significantly decreased in the 4th week after induction of diabetes by STZ compared to the 0th week in diabetic groups.

Table 3. Levels of blood biochemical parameters at the 0th, 4th and 8th weeks in the experimental groups.

Groups	Time (weeks)	Glucose (mg/dL)	Cr (µmol/L)	BUN (mg/dL)	HDL (mmol/L)	MDA (µmol/L)	LDL (mg/dL)	TG (mg/dL)
Group A (normal)	0	80.11 ± 2.41	44.14 ± 1.23	12.43 ± 1.53	84.52 ± 5.32	0.76 ± 0.01	38.12 ± 2.4	65.23 ± 5.22
	4	85.21 ± 9.07	50.23 ± 2.24	14.83 ± 0.61	86.12 ± 3.21	0.82 ± 0.03	36.05 ± 2.11	70.5 ± 1.52
	8	83.142 ± 3.51^{bcde}	53.12 ± 4.62^{bcde}	16.82 ± 0.45^{bcde}	88.11 ± 2.56^{bde}	0.74 ± 0.04^{bcde}	31.32 ± 1.42^{bcde}	68.25 ± 2.31^{bcde}
Group B (control)	0	89.62 ± 5.12	47.21 ± 4.21	14.41 ± 2.11	88.45 ± 5.32	0.55 ± 0.01	35.72 ± 7.11	61.32 ± 4.81
	4	375.43 ± 4.62$^{\#}$	115.11 ± 8.11$^{\#}$	33.33 ± 0.21$^{\#}$	35.53 ± 1.24$^{\#}$	3.16 ± 0.03$^{\#}$	71.12 ± 4.62$^{\#}$	229.75 ± 5.31$^{\#}$
	8	387.42 ± 5.3 3$^{\#acde}$	117.36 ± 1.64$^{\#acde}$	49.38 ± 0.22$^{\#acde}$	33.22 ± 4.44$^{\#}$	3.63 ± 0.06$^{\#ac}$	68.94 ± 5.32$^{\#acde}$	256.75 ± 3.83 $^{\#acde}$
Group C (insulin)	0	77.35 ± 6.61	34.11 ± 2.53	12.24 ± 1.34	83.74 ± 6.11	0.44 ± 0.02	39.22 ± 4.24	61.34 ± 5.23
	4	352.72 ± 3.41$^{\#}$	122.94 ± 2.81$^{\#}$	32.88 ± 0.33$^{\#}$	46.64 ± 4.32$^{\#}$	1. 81 ± 0.66$^{\#}$	74.96 ± 4.22$^{\#}$	247.75 ± 4.61$^{\#}$
	8	305.22 ± 6.21$^{*\#ab}$	81.77 ± 4.72$^{*\#ab}$	17.56 ± 0.23$^{*\#ab}$	72.21 ± 1.62^{*bd}	1.05 ± 0.23$^{*\#abd}$	46.11 ± 1.1^{*ab}	202.4 ± 4.66$^{*\#ab}$
Group D (PIO)	0	84.11 ± 7.33	40.72 ± 4.71	13.52 ± 2.12	85.23 ± 7.23	0.51 ± 0.04	44.11 ± 6.25	58.11 ± 4.44
	4	376.22 ± 7.26$^{\#}$	118.11 ± 5.43$^{\#}$	35.92 ± 0.22$^{\#}$	38.28 ± 1.43$^{\#}$	3.11 ± 0.81$^{\#}$	79.23 ± 1.16$^{\#}$	244.91 ± 5.23$^{\#}$
	8	334.21 ± 4.23$^{*\#abe}$	87.11 ± 4.22$^{*\#ab}$	26.16 ± 0.63$^{*\#abe}$	51.05 ± 2.72$^{*\#abe}$	2.01 ± 0.32$^{*\#abce}$	49.24 ± 2.32^{*abe}	214.62 ± 6.8$^{*\#abe}$
Group E (PIO-MS)	0	75.34 ± 7.43	37.43 ± 5.22	15.6 ± 1.43	76.1 ± 6.64	0.06 ± 0.01	33.72 ± 3.34	61.06 ± 6.14
	4	364.31 ± 4.11$^{\#}$	134.21 ± 5.61$^{\#}$	32.51 ± 0.11$^{\#}$	36.22 ± 2.11$^{\#}$	3.20 ± 0.52$^{\#}$	75.50 ± 3.23$^{\#}$	247.6 ± 6.11$^{\#}$
	8	319.15 ± 3.53$^{*\#abd}$	89.11 ± 5.43$^{*\#ab}$	19.29 ± 0.61^{*abd}	64.47 ± 4.23^{*abd}	1.22 ± 0.71$^{*\#abd}$	46.36 ± 1.52^{*abd}	205.81 ± 6.56$^{*\#abd}$

Data were shown as Mean ± SD. Paired T-Test was used to compare differences between weeks in each group. $^{\#}P < 0.05$ shows significant difference compared to the 0th week; $^{*}P < 0.05$ versus the 4th week. ANOVA was used to compare differences in the 8th week among groups. $^{a}P < 0.05$ indicates significant difference compared to normal group; $^{b}P < 0.05$ versus control group; $^{c}P < 0.05$ versus insulin group (positive control); $^{d}P < 0.05$ versus PIO group; $^{e}P < 0.05$ versus PIO-MS group. PIO, Pioglitazone; PIO-MS, pioglitazone-loaded mesoporous silica.

The level of MDA in the control group was significantly different from the insulin group. Moreover, the comparison between before (4th week) and after (8th week) treatment in insulin and PIO groups revealed decreasing in MDA, significantly. The level of MDA decreased in the PIO-MS group significantly compared with the PIO group.

The parameters decreased in PIO and insulin groups compared with the control group, significantly. Furthermore, the serum levels of BUN, TG, LDL, and blood glucose significantly decreased in the PIO-MS group in comparison with the PIO group.

HDL level significantly decreased in diabetic rats in comparison between 0th and 4th weeks, yet its level increased in drug therapy groups (8th week) considerably compared to before treatment (4th week). Furthermore, the PIO-MS group meaningfully had increased HDL levels compared with the PIO group.

The Cr level decreased in PIO and insulin groups compared with the control group, significantly.

Renal histology and morphometric analysis

Glomeruli were effortlessly recognized by their characteristic circular morphological part of the peripheral lumen. Figure 6 showed representative histopathological changes in the kidney with H & E staining.

The enlargement of the glomerular, moderate to severe enlargement of the mesangial matrix, the thickening of basement membrane and, vascular wall, the narrowing of capillary space, and the attachment of the glomerular plexus to Bowman capsule were observed in the control group compared with the normal group.

In the insulin group, the reduction in glomerular size was as close as normal, with a slight to moderate increase in the mesangial matrix and the presence of Bowman's capsule adhesion to the glomerulus.

A moderate decrease in glomerular size, a slight increase in the mesangial matrix, and the presence of Bowman's capsule in the glomerulus were observed in the PIO-MS group.

A moderate increase in the mesangial matrix, a minimal decrease in glomerular size, and Bowman's capsule adhesion to the glomerulus were observed in the PIO group.

DISCUSSION

Diabetes is associated with both microvascular and macrovascular complications (8). The American Diabetes Association defined diabetes mellitus (DM) as a metabolic disease characterized by hyperglycemia resulting from defects in insulin secretion, insulin action, or both. The chronic hyperglycemia of diabetes is associated with long-term damage, dysfunction, and failure of different organs, especially the eyes, kidneys, nerves, heart, and blood vessels. Pioglitazone is a Food and Drug Administration-approved TZD derivative and PPARγ agonist and used for the treatment of DM (8).

The present study was designed to evaluate the effect of pioglitazone on STZ-induced diabetes in rats regarding their effect on blood glucose, lipid profile, and kidney function. This drug is not highly soluble and can be effective in the amount of absorbed drug; therefore, mesoporous systems were first used as solubility enhancers (22). At first, carriers were prepared to increase drug solubility with different surfactants to prepare MS and MA systems. When mesoporous particles are loaded with a drug, the drug signal confirms that there is no interference between materials in any of the formulations (MS and MA). The FTIR diagram of the calcined porous MS and MA was consistent with Chen's (18) and More's studies (23).

By increasing the amount of surfactant, the loading rate of the drug in the mesoporous cavities increased, which may be related to the many pores made; consequently, the release rate of the drug from the cavities increased. Formulations containing 1.5 g of surfactant showed more drug loading and release than formulations containing 0.5 g of surfactant, as shown in Fig. 5.

The uniform and nano-size of the particles also were seen in SEM-related images and made them suitable and desirable. The nanoparticles increased the surface area that increased the contact surface of the drug with the available solvent, resulting in increased solubility and could be effortlessly released from the mesoporous structure, and increased the dissolution rate. The difference in results between SEM and Zetasizer was related to the difference in the hydrodynamic diameter of the particles.

The XRD pattern of pioglitazone showed that it was highly crystalline as indicated by the numerous sharp peaks, and when loaded into MS, they can retain their crystallinity. Exhibiting high crystallinity after drug loading in mesoporous refers to the ability of the drug molecules to form well-defined crystal structures within the pores of the silica and alumina materials (24). This is desirable as it can enhance the stability, controlled release, and therapeutic efficacy of the drug. When the drug molecules are loaded into the pores, they can experience a confined environment that promotes their organization and crystallization (25). The drug molecules may interact with the surface of the silica material through various forces such as hydrogen bonding, electrostatic interactions, or van der Waals forces. These interactions can lead to the alignment and ordering of the drug molecules within the pores, resulting in a highly crystalline structure (26). The stability and compatibility of the drug with the MS material can also play a role in maintaining the crystalline structure (27). Crystallinity was seen after loading in MS and MA nanoparticles.

PDI is an essential indicator for showing the uniform size of nanoparticles, and the results indicated a small PDI (Table 1). The low PDI was desirable because higher stability occurred, and suspended particles were less likely to accumulate.

The positive or negative zeta potential of suspended particles prevents the accumulation of particles (28). It is known that the solids with stable surfaces can produce zeta potential between -30 and -50 mV in deionized water at neutral pH (29). Negative zeta potential is another factor showing that the manufactured nanoparticles are stable. Both MS and MA had a negative zeta potential value, indicating that the post-synthesis suspensions were stable, and the negative charge was because of the silanol and hydroxyl groups. The results were consistent with Luo's study (30) (zeta potential of -30.7 mV) and Das's study (31) (zeta potential between -27 and -48 mV).

In general, MS particles showed a smaller particle size compared to MA particles. In addition, the particles had highly loaded and released drugs. Based on the *in vitro* results including smaller size, more drug loading and releasing, and no interference between materials, MS with more surfactant (1.5 g CTAB) was evaluated for *in vivo* experiments.

The investigation of physical factors in animals presented that the groups receiving insulin and pioglitazone could increase the weight of animals. Our results is in line with the findings of Ko *et al*. (32) and Hirasawa *et al.* (33) who demonstrated dose-related weight gain in studies performed on pioglitazone in diabetic nephropathy probably due to fat accumulation.

The major cation in intracellular fluid is potassium, while the major cation in the extracellular fluid is sodium (34). Increased urinary sodium and potassium indicate renal failure (35). The groups receiving the treatment showed that the factors measured in the urine improved and the results of other studies confirm this finding. According to Ko (32), and Afzal's (35) studies, diabetic rats treated with 30 mg/kg pioglitazone had a significant decrease in urine volume compared with diabetic rats with no treatments.

MS containing drugs significantly showed a decrement in urinary parameters, TG, LDL, BUN, blood glucose, MDA, and Cr, and an increment in HDL. Studies attempted to find the effects of pioglitazone on biochemical factors in diabetic rats, which represented the improvement in the factors in rats receiving pioglitazone (36,37). The current research revealed that the rats receiving pioglitazone loaded in nanoparticles mesopore provided a significant increase in the improvement of biochemical elements compared with rats receiving pioglitazone alone. Several researchers reported increased levels of MDA in the renal tissues of diabetic rats because of oxidative stress and the indirect evidence of free radical production (36-38). The constant generation of free radicals could prompt tissue damage by assaulting membranes through the peroxidation of unsaturated fatty acids (33). Some shreds of evidence also found that pioglitazone could reduce MDA, indicating the anti-inflammatory effects of pioglitazone (8,33,39). The decreased levels of lipid peroxidation might be one of the mechanisms by which drug treatment could contribute to preventing diabetic complications (40). Bahriz *et al*. demonstrated that pioglitazone administered by gastric gavage for 4 weeks produced more improvement in LDL, TG, BUN, Cr, and MDA levels in diabetic rats (8). Moreover, another study reported that pioglitazone improved the levels of glucose, cholesterol, Cr, and TG in diabetic nephropathy (32). Based on other studies performed on diabetic animal models, pioglitazone (30 mg/kg/day) can reduce the levels of MDA and Cr (41), as well as decrease the serum levels of BUN and TG, and increase the levels of HDL (42).

The current research performed a histological investigation on kidney tissues to confirm the results. The investigation indicated that the size of glomeruli and other substantial parameters in the group receiving pioglitazone loaded in nanoparticles could significantly decrease, and reach the normal size. In line with current findings, other documents reported that the effect of pioglitazone on kidney tissue caused an identical effect as well as the same dose of pioglitazone (33,42,43).

CONCLUSION

Synthesized MA and MS efficiently loaded the pioglitazone, leading to an enhanced dissolution rate compared with the pure crystalline drug. According to the current study results, PIO-MS may prevent the development of diabetic nephropathy as well as improve hyperlipidemia and remarkable kidney function parameters. The findings suggest that PPARγ agonist ameliorates diabetic nephropathy through anti-inflammatory mechanisms in type 1 diabetic rats. However, larger-scale investigations are demanded to determine its effect on diabetic nephropathy. It is recommended to measure the effectiveness of pioglitazone loaded in MA nanoparticles on a diabetic animal model and compare it with the present study findings.

Acknowledgments

There was no financial support.

Conflicts of interest statement

The authors declare no conflict of interest, financial or otherwise.

Authors' contributions

S. Ahmadipour was involved in supervising, providing the facilities and experimental design, verifying the analytical methods, and consulting in writing the manuscript; A. Dezhangfard performed the experiments, analyzed the data, and wrote the manuscript; J. Varshosaz provided the facilities and experimental design, verified the analytical methods, and consulting in writing the manuscript. All authors read and approved the final version of the manuscript.

REFERENCES

1. Saeedi P, Petersohn I, Salpea P, Malanda B, Karuranga S, Unwin N, *et al*. Global and regional diabetes prevalence estimates for 2019 and projections for 2030 and 2045: results from the International Diabetes Federation Diabetes Atlas, 9th edition. Diabetes Res Clin Pract. 2019;157: 107843,1-10. DOI: 10.1016/j.diabres.2019.107843.
2. Johansen KL, Chertow GM, Foley RN, Gilbertson DT, Herzog CA, Ishani A, *et al*. US renal data system 2020 annual data report: epidemiology of kidney disease in the United States. Am J Kidney Dis. 2021;77(4):A7-A8. DOI: 10.1053/j.ajkd.2021.01.002.
3. Widowati W, Tjokropranoto R, Onggowidjaja P, Kusuma HSW, Wijayanti CR, Marthania M, *et al*. Protective effect of yacon leaves extract (*Smallanthus sonchifolius* (Poepp.) H. Rob) through antifibrosis, anti-inflammatory, and antioxidant mechanisms toward diabetic nephropathy. Res Pharm Sci. 2023;18(3):336-345. DOI: 10.4103/1735-5362.371589.
4. Choudhury D, Tuncel M, Levi M. Diabetic nephropathy-a multifaceted target of new therapies. Discov Med. 2010;10(54):406-415. PMID: 21122472.
5. Troncoso Brindeiro CM, Fallet RW, Lane PH, Carmines PK. Potassium channel contributions to afferent arteriolar tone in normal and diabetic rat kidney. Am J Physiol Renal Physiol. 2008;295(1):F171-F178. DOI: 10.1152/ajprenal.00563.2007.
6. Lebovitz HE. Thiazolidinediones: the forgotten diabetes medications. Curr Diab Rep. 2019;19(12):151,1-3. DOI: 10.1007/s11892-019-1270-y.
7. Motoki T, Kurobe H, Hirata Y, Nakayama T, Kinoshita H, Rocco KA. PPAR-γ agonist attenuates inflammation in aortic aneurysm patients. Gen Thorac Cardiovasc Surg. 2015; 63:565–571. DOI: 10.1007/s11748-015-0576-1.
8. Bahriz A, Ismaiel Y, Abdelhameed A, Elsayed F. Effect of sitagliptin, pioglitazone and dapagliflozine on myocardial infarction induced experimentally in diabetic rats. Benha Med J. 2021;38(Academic issue):147-165. DOI: 10.21608/BMFJ.2021.146796.
9. Maciejewska-Skrendo A, Massidda M, Tocco F, Leźnicka K. The influence of the differentiation of genes encoding peroxisome proliferator-activated receptors and their coactivators on nutrient and energy metabolism. Nutrients. 2022;14(24):5378, 1-28. DOI: 10.3390/nu14245378.
10. Faiz S, Arshad S, Kamal Y, Imran S, Asim MH, Mahmood A, *et al*. Pioglitazone-loaded nanostructured lipid carriers: *in-vitro* and *in-vivo* evaluation for improved bioavailability. J Drug Deliv Sci Technol. 2023;79:104041. DOI: 10.1016/j.jddst.2022.104041.
11. Varshosaz J, Ahmadipour S, Tabbakhian M, Ahmadipour S. Nanocrystalization of pioglitazone by precipitation method. Drug Res. 2018;68(10):576-583. DOI: 10.1055/a-0591-2506.
12. Wang Z, Du H, Zhao Y, Ren Y, Ma C, Chen H, *et al*. Response to pioglitazone in non-alcoholic fatty liver disease patients with vs. without type 2 diabetes: a meta-analysis of randomized controlled trials. Front Endocrinol. 2023;14:1111430,1-11. DOI: 10.3389/fendo.2023.1111430.
13. Mirzaei M, Babaei Zarch M, Darroudi M, Sayyadi K, Keshavarz ST, Sayyadi J, *et al*. Silica mesoporous structures: effective nanocarriers in drug delivery and nanocatalysts. Appl Sci. 2020;10(21):7533,1-36. DOI: 10.3390/app10217533.
14. Hu Y, Wang J, Zhi Z, Jiang T, Wang S. Facile synthesis of 3D cubic mesoporous silica microspheres with a controllable pore size and their application for improved delivery of a water-insoluble drug. J Colloid Interface Sci. 2011;363(1):410-417. DOI: 10.1016/j.jcis.2011.07.022.
15. Mellaerts R, Aerts CA, Van Humbeeck J, Augustijns P, Van den Mooter G, Martens JA. Enhanced release of itraconazole from ordered mesoporous SBA-15 silica materials. Chem Commun. 2007;13:1375-1377. DOI: 10.1039/B616746b.
16. Varshosaz J, Dayani L, Chegini SP, Minaiyan M. Production of a new platform based on fumed and mesoporous silica nanoparticles for enhanced solubility and oral bioavailability of raloxifene HCl. IET Nanobiotechnol. 2019;13(4):392-399. DOI: 10.1049/iet-nbt.2018.5252.
17. Grant SM. Polymer templating synthesis, adsorption and structural properties of alumina-based ordered mesoporous materials. Ph.D. [Thesis]. Kent: Kent State University , 2011. Available online: http://rave.ohiolink.edu/etdc/view?acc_num=kent1317593306 (accessed on 31 January 2023).
18. Chen B, Wang Z, Quan G, Peng X, Pan X, Wang R, *et al*. *In vitro* and *in vivo* evaluation of ordered mesoporous silica as a novel adsorbent in liquisolid formulation. Int J Nanomedicine. 2012;7:199-209. DOI: 10.2147/IJN.S26763.
19. Ahmadipour S, Varshosaz J, Hashemibeni B, Safaeian L, Manshaei M. Polyhedral oligomeric silsesquioxane /platelets rich plasma/gelrite-based hydrogel scaffold for bone tissue engineering. Curr Pharm Des. 2020;26(26):3147-3160.

DOI: 10.2174/1381612826666200311124732.
20. Ebaid H, Bashandy SAE, Abdel-Mageed AM, Al-Tamimi J, Hassan I, Alhazza IM. Folic acid and melatonin mitigate diabetic nephropathy in rats *via* inhibition of oxidative stress. Nutr Metab (Lond). 2020;17(1):1-14.
DOI: 10.1186/s12986-019-0419-7.
21. Furman BL. Streptozotocin-induced diabetic models in mice and rats. Curr Protoc Pharmacol. 2021;70(5):47,1-5.
DOI: 10.1002/0471141755.ph0547s70.
22. Le TT, Elzhry Elyafi AK, Mohammed AR, Al-Khattawi A. Delivery of poorly soluble drugs *via* mesoporous silica: impact of drug overloading on release and thermal profiles. Pharmaceutics. 2019;11(6):269,1-16.
DOI: 10.1016/j.sjbs.2016.01.010.
23. More MP, Ganguly PR, Pandey AP, Dandekar PP, Jain RD, Patil PO, *et al*. Development of surface engineered mesoporous alumina nanoparticles: drug release aspects and cytotoxicity assessment. IET Nanobiotechnol. 2017;11(6):661-668.
DOI: 10.1049/iet-nbt.2016.0225.
24. Slowing II, Trewyn BG, Giri S, Lin VS. Mesoporous silica nanoparticles for drug delivery and biosensing applications. Adv Funct Mater. 2008;17(8):1225-1236.
DOI: 10.1002/adfm.200601191.
25. Zhao Y, Sun X, Zhang G, Trewyn BG. Dendrimer-templated mesoporous silica nanoparticles for pH-responsive drug delivery. Chem Commun (Camb). 2011;47(12):3332-3334.
DOI: 10.1039/c0cc05188k.
26. Slowing II, Vivero-Escoto JL, Wu CW, Lin VS. Mesoporous silica nanoparticles as controlled release drug delivery and gene transfection carriers. Adv Drug Deliv Rev. 2008;60(11):1278-1288.
DOI: 10.1016/j.addr.2008.03.012.
27. Rosenholm JM, Sahlgren C, Lindén M. Towards multifunctional, targeted drug delivery systems using mesoporous silica nanoparticles-opportunities & challenges. Nanoscale. 2010;2(10):1870-1883.
DOI:10.1039/c0nr00156b.
28. Vazquez NI, Gonzalez Z, Ferrari B, Castro Y. Synthesis of mesoporous silica nanoparticles by sol-gel as nanocontainer for future drug delivery applications. Bol Soc Esp Ceram Vidr. 2017;56(3):139-145.
DOI: 10.1016/j.bsecv.2017.03.002.
29. Vaisman L, Marom G, Wagner HD. Dispersions of surface-modified carbon nanotubes in water-soluble and water-insoluble polymers. Adv Funct Mater. 2006;16(3):357-363.
DOI: 10.1002/adfm.200500142.
30. Luo GF, Chen WH, Liu Y, Lei Q, Zhuo RX, Zhang XZ. Multifunctional enveloped mesoporous silica nanoparticles for subcellular co-delivery of drug and therapeutic peptide. Sci Rep. 2014;4(1):1-10.
DOI: 10.1038/srep06064.
31. Das D, Yang Y, O'Brien JS, Breznan D, Nimesh S, Bernatchez S, *et al*. Synthesis and physicochemical characterization of mesoporous nanoparticles. J Nanomater. 2014;2014:62,1-12.
DOI: 10.1155/2014/176015.
32. Ko GJ, Kang YS, Han SY, Lee MH, Song HK, Han KH, *et al*. Pioglitazone attenuates diabetic nephropathy through an anti-inflammatory mechanism in type 2 diabetic rats. Nephrol Dial Transplant. 2008;23(9):2750-2760.
DOI: 10.1093/ndt/gfn157.
33. Hirasawa Y, Matsui Y, Yamane K, Yabuki SY, Kawasaki Y, Toyoshi T, *et al*. Pioglitazone improves obesity type diabetic nephropathy: relation to the mitigation of renal oxidative reaction. Exp Anim. 2008;57(5):423-432.
DOI: 10.1538/expanim.57.423.
34. Yamada S, Inaba M. Potassium metabolism and management in patients with CKD. Nutrients. 2021;13(6):1751,1-19.
DOI: 10.3390/nu13061751.
35. Afzal S, Sattar MA, Johns EJ, Eseyin OA. Renoprotective and haemodynamic effects of adiponectin and peroxisome proliferator-activated receptor agonist, pioglitazone, in renal vasculature of diabetic spontaneously hypertensive rats. PloS One. 2020;15(11):e0229803,1-22.
DOI: 10.1371/journal.pone.0229803.
36. Manzano M, Colilla M, Vallet-Regí M. Drug delivery from ordered mesoporous matrices. Expert Opin Drug Deliv. 2009;6(12):1383-1400.
DOI: 10.1517/17425240903304024.
37. Zhang Y, Wang J, Bai X, Jiang T, Zhang Q, Wang S. Mesoporous silica nanoparticles for increasing the oral bioavailability and permeation of poorly water soluble drugs. Mol Pharm. 2012;9(3):505-513.
DOI: 10.1021/mp200287c.
38. Colilla M, Manzano M, Izquierdo-Barba I, Vallet-Regí M, Boissiére C, Sanchez C. Advanced drug delivery vectors with tailored surface properties made of mesoporous binary oxides submicronic spheres. Chem Mater. 2010;22(5):1821-1830.
DOI: 10.1021/cm9033484.
39. Karabas MK, Ayhan M, Guney E, Serter M, Meteoglu I. The effect of pioglitazone on antioxidant levels and renal histopathology in streptozotocin-induced diabetic rats. ISRN Endocrinol. 2013;2013:858690,1-8.
DOI: 10.1155/2013/858690.
40. Rao PS, Mohan GK. *In vitro* alpha-amylase inhibition and *in vivo* antioxidant potential of *Momordica dioica* seeds in streptozotocin-induced oxidative stress in diabetic rats. Saudi J Biol Sci. 2017;24(6):1262-1267.
DOI: 10.1016/j.sjbs.2016.01.010.
41. Attallah MI, Ibrahim AN, Elnaggar RA. Effects of pioglitazone and irbesartan on endothelial dysfunction on experimentally streptozotocin-induced diabetic nephropathy in rats. Egypt J Basic Clin Pharmacol. 2018;8(3):1-14.
DOI: 10.11131/2018/101368.
42. Cao YH, Kuang L, Dai W, XingY, Ye SD. Effect of pioglitazone on the expression of renal tissue nephrin in STZ-induced diabetic rats. Int J Clin Exp Pathol. 2016;9(2):1676-1683.
DOI: 10.1371/journal.pone.0264129.
43. Peng XH, Liang PY, Ou SJ, Zu XB. Protective effect of pioglitazone on kidney injury in diabetic rats. Asian Pac J Trop Med. 2014;7(10):819-822.
DOI: 10.1016/S1995-7645(14)60143-7.